**"A Cochlear Nucleus Auditory**

**Prosthesis based on microstimulation”**

Contract No. **No. NO1-DC-4-0005**
Progress Report #11

**HUNTINGTON MEDICAL RESEARCH INSTITUTES**
NEURAL ENGINEERING LABORATORY
734 Fairmount Avenue
Pasadena, California 91105

D.B. McCreery, PhD
---
---
**HOUSE EAR INSTITUTE**
2100 WEST THIRD STREET
Los Angeles, California 90057
---
R.V. Shannon, PhD
Steve Otto, MS

SUMMARY AND ABSTRACT

I: Activities at Huntington Medical Research Institutes

Part of the work scope this project is to objectively compare the ability of penetrating microstimulating electrodes and surface macroelectrodes to selective access the tonotopic organization of the ventral cochlear nucleus. We have used a modified version of our microstimulating cochlear nucleus arrays, with 16 microstimulating sites on 4-shanks, and with 2 surface macroelectrodes (geometric area of approximately 0.4 $mm^{2)}$ on the under surface of the array superstructure. During the past quarter, these modified arrays were implanted chronically into three cats, and responses in the inferior colliculus were recorded during terminal experiments in two of these. Data from one animal were considered unreliable due to elevated neural response thresholds and other evidence that the array's silicon had been damaged during insertion.

In cat CN165, multiunit neuronal activity was recorded at 16 sites along the tonotopic gradient of the central nucleus of the contralateral inferior colliculus (ICC), while stimulating in the contralateral ventral cochlear nucleus with either the surface electrodes or the intranuclear microelectrodes. The spectral selectivity of the surface electrodes and penetrating microelectrodes was quantified according to the relation between the amount of induced neuronal activity and the distribution of the activity along the tonotopic gradient of the ICC. By this measure, the neural activity induced by the penetrating microstimulating electrodes was more restricted along the tonotopic gradient of the ICC than was the activity from the small surface electrodes when the total neuronal activity was high, but the spatial selectivity of the surface and penetrating electrodes was comparable near the response threshold. In this animal, the spectral selectivity of the surface electrode was greater than in the animals reported in the pervious report, in which the stimulating array was implanted acutely, just before the measurements in the ICC. This difference probably can be attributed to the tendency for the growth of connective tissue under and around the chronically-implanted array superstructure to restrict the spread of the stimulus current from the surface electrode. The latencies of the responses induced in the ICC were significantly different for the surface and microelectrodes, suggesting that they were activating different neuronal pathways from the cochlear nucleus to the ICC.

**II Activities at the House Ear Institute**

Nine patients have now received the PABI device and are using it in daily life. Four have no auditory sensations on the penetrating electrodes and so only use the surface electrodes. The patients have auditory percepts on surface electrodes and on only one penetrating electrode. All other penetrating electrodes produce either no percept or an undesirable non-auditory percept. Two patients have diverse auditory percepts on multiple penetrating electrodes, which they use in combination with surface electrodes in their processors. There is so far no clear evidence of an advantage of penetrating electrodes in speech recognition performance.

**I: Work at Huntington Medical Research Institutes**

**Comparisons of spectral specificity of micro-and macrostimulating electrodes in the cat cochlear nucleus.**

Part of the work scope of our contract call for us to objectively compare the ability of penetrating microstimulating electrodes and surface macroelectrodes to selective access the tonotopic organization of the ventral cochlear nucleus. This work was begun in the previous quarter and we continued this study in the last quarter, using similar methods.

We have used a modified version of the microstimulating arrays with 16 stimulating sites on 4-shanks, and with 2 macroelectrodes on the under surface. Figure 1A shows a multisite silicon substrate probe with 2 shanks and 8 stimulating sites sputter-coated with iridium oxide. The probes were fabricated at the University of Michigan under the direction of Design Engineer Jamille Hetke, and provided to us through NeuroNexus, Inc. The 4 electrode sites on each shank are 0.8 to 1.7 mm below the probe's transverse spine. After bonding of the Parylene-coated gold lead wires, the transverse spines of two probes were encapsulated in EpoTek 301 epoxy to form the button superstructure, 2.5 mm in diameter. The 8 or 16 lead wires were wound into a helical cable and encapsulated in silicone elastomer. A complete array of 2 probes (4 shanks and 16 electrode sites) extending from the epoxy superstructure is shown in figure 1B.

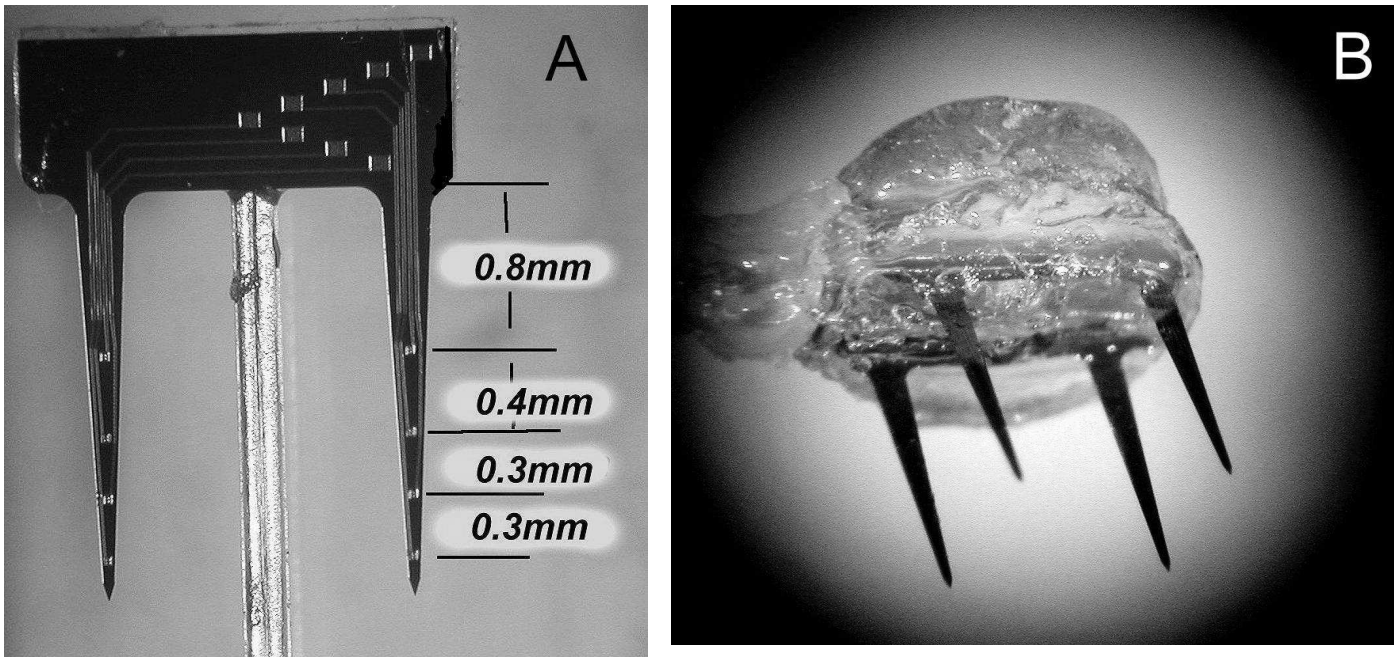


Figure 1

The rectangular platinum macroelectrodes (surface electrodes) have a geometric area of approximately 0.4 $mm^2$, as in the surface array now used in the clinical auditory brainstem implant (ABI) program. These are set between the silicon shanks, which in figure 2 are oriented towards the camera. The array superstructure is implanted on the dorsolateral surface of the cochlear nucleus, with one macroelectrode dorsal and medial and the second ventral and lateral, so that the medial macroelectrode will have a chance to access the high acoustic frequencies and the lateral electrode will access low frequencies. The silicon shanks penetrate into the ventral cochlear nucleus. In our cat model, the spread of neuronal activity along the tonotopic gradient of the ventral cochlear nucleus is quantified as the spread of activity along the dorsolateral-ventromedial axis of the central nucleus of the inferior colliculus, using the methods described in our pervious quarterly reports, and summarized below

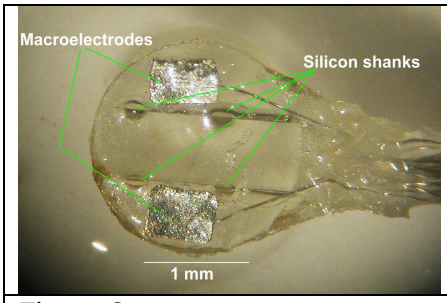

Figure 2

.

In the studies conducted in the past quarter, the stimulating arrays were implanted in the ventral CN for 18 or 24 days, while those conducted in the previous quarter and reported in QPR #10 employed stimulating arrays implanted acutely into the CN, a few hours before the start of data acquisition. Otherwise, the methods were very similar. For implantation of the stimulating array, a craniectomy was made over the cerebellum on the right side and part of the lateral cerebellum was aspirated. The array superstructure was retained against the orifice of a vacuum wand, and advanced into the CN at approximately 45$^{o}$ from the vertical; approximately the angle at which a microelectrode array would be inserted into the human CN, using the translabyrinthine approach to brainstem. The array cable was fixed to the bone at the margin of the craniectomy, the cavity was filled with gelfoam, and the bone defect sealed with bone cement. The recordings from the inferior colliculus were terminal, non-recovery experiments. The cats were anesthetized with Isoflurane and oxygen, and their heads fixed in a stereotaxic frame. To facilitate delivery of acoustic stimuli, a hollow earbar was used contralateral to the inferior colliculus from which recordings were made. The ipsilateral earbar was solid, in order to attenuate acoustic stimuli. A wide craniectomy was made over the left cerebral hemisphere, and the occipital pole of the cerebrum was removed to expose the dorsal surface of the inferior colliculus. The cat was transferred to a double-wall sound isolation booth (Audiometrics 120A-SP).Throughout the experiment, respiration rate and end-tidal $CO_2$ were monitored continuously. Core body temperature was maintained at 37-39℃

The tonotopic organization of the anteroventral and posteroventral CN is preserved in the projection from the CN to the ICC, where the iso-frequency laminae are oriented approximately perpendicular to its dorsolateral-ventromedial (DLVM) axis, with low acoustic frequencies represented dorsally and laterally and high frequencies represented ventrally and medially. Multiunit neuronal activity was recorded at 16 locations separated by 200 μm and spanning 3 mm along the DLVM axis of ICC, using a multisite probe fabricated by NeuroNexus, Inc. For each insertion of the recording probe, the representation of acoustic frequencies in the ICC was mapped using tone bursts ranging from 0.5 to 25 kHz, and 40 ms in duration with a rise time of 10 ms. These were delivered through a broad-band loudspeaker (~ ±5 db, 200 Hz to 35 kHz).

After the acoustic mapping, 1500 controlled-current, biphasic stimulus pulses (150 μs/ph in duration at 50 pps) were applied to each of the microelectrode sites in the CN. Extracellular action potentials (multiunit activity, MUA) evoked in the ICC by the stimulation in the VCN were separated from the large compound response using a common background suppression technique and bandpass filtering between 500 Hz and 8 kHz. Action potentials were sorted into bins 100 μs in width and summed over the 1500 presentation of the stimulus, yielding 16 PST (post-stimulus time) histograms, one PST for each recording site in the ICC. The 16 histograms represent, in PST and depth in the ICC, the MUA evoked in response to the stimulation in the VCN. Response maps of the MUA in post-stimulus time and depth in the ICC were generated from the 16 PST histograms. These maps are analogous to the response images in time and position recorded in the cerebral cortex of the guinea (Arenberg et al, 2000, Bierer and Middlebrooks, 2002). The time and depth co-ordinates of the activity centroids were computed as the means, in depth in the ICC and PST, of the counts of the MUA from the bins comprising the maps. Computation of the maps' centroids can be seriously skewed by MUA that is far from the maximum neuronal response to the electrical stimulus in the VCN. This background activity is present in most of the bins of the PST histograms, but it contributes only a few counts to each histogram bin. Thus the centroids were generated only from histograms bins in which the spike count was at least 50% of the "averaged maximum count" (AMC) (Arenberg et al, 2000). The histogram's maxima is well defined by the average of the counts in the 4 bins ( the 400 ms window) around the peak, so we computed this 4-bin average for each of the 16 histograms and selected the largest of these as the AMC. This procedure also takes into account the fact that the span of the feline ICC is greater than the span of the recording array. By computing the centroids only from the bins that are fairly close to the 4 bins contributing to the AMC, we also reduce "edge artifact" whereby centroids near the upper or lower extremes of the recording array tend to be computed as being closer to the center

of the array than is actually the case.

Neuronal activity induced from a particular simulating electrode in the CN was quantified as the total number of extracellular spikes all 16 PST histograms ("total neuronal activity"). The spread of neuronal activity above and below the depth co-ordinate of the centroid in the ICC was quantified as the square root of the second central moment of the distribution of the neuronal activity about the depth co-ordinate of the centroid (along the axis of recording probe). This is mathematically identical to the standard deviation of the distribution of the activity about the mean, a commonly-used measure of the dispersion of a distribution function. Here it is designated as "dispersion of neuronal activity". To reduce the influence of background spike activity on this computation, only bins from the PST histogram in which the activity was at least 10% of the AMC were used. As with acoustic stimuli and intracochlear stimulation (Snyder et al, 2004) both dispersion of neuronal activity and total neuronal activity vary with stimulus amplitude, and so spectral dispersion was quantified as the ratio of dispersion of the activity to total activity. Dispersion of activity and total activity were computed for the first 50 presentations of the stimulus at each stimulating site in the CN ("on transient response") and for stimulus pulses 200 through 1500 ("steady-state response").

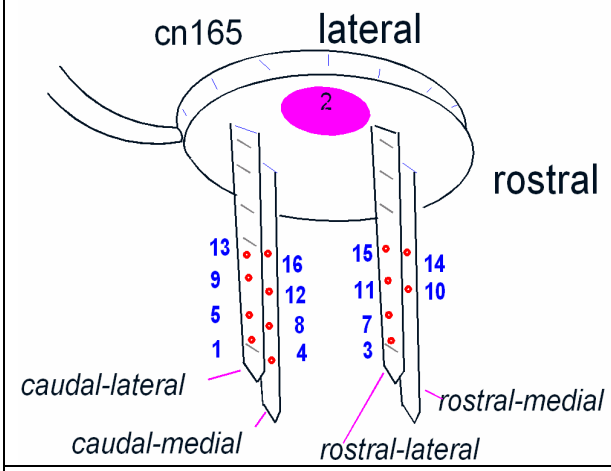


Figure 3A

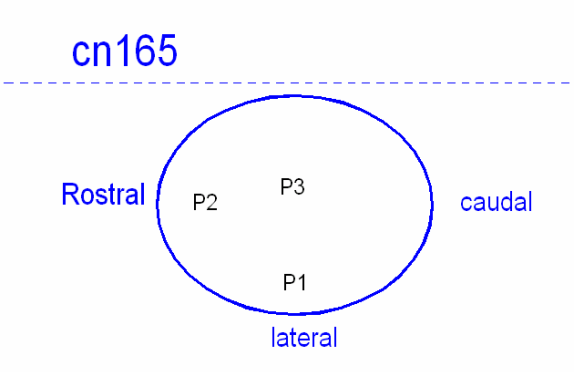


Figure 3B

RESULTS.

During the past quarter, these modified arrays were implanted chronically into three cats, and responses in the inferior colliculus were recorded during terminal experiments in two of these. Data from one animal (CN164) were considered unreliable due to elevated neural response thresholds and other evidence that the array's silicon had been damaged during insertion. In CAT 165, the response thresholds from the intranuclear microstimulating electrodes were low ( 5-15 µA) and the electrical measurements from the stimulating array were nominal. Figure 3A depicts the location of the 12 available microstimulating sites on the shanks of the array implanted for 24 days in the right cochlear nucleus of cat CN165. The histology from this animal is pending, but the location of the array's superstructure on the dorsal surface of the CN indicates that the caudal shanks were in the caudal posteroventral cochlear nucleus and the rostral shanks were in the rostral part of the PVCN. Figure 3B depicts the 3 points on the surface of the inferior colliculus at which the recording array was inserted through the pia. The probe then was inserted down into the central nucleus (ICC) at an angle of 45° from the vertical.

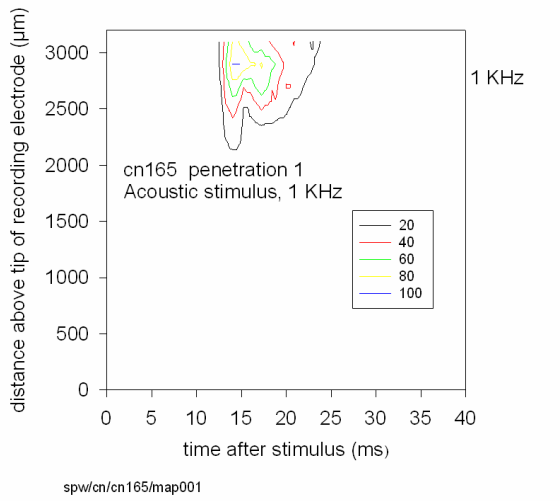


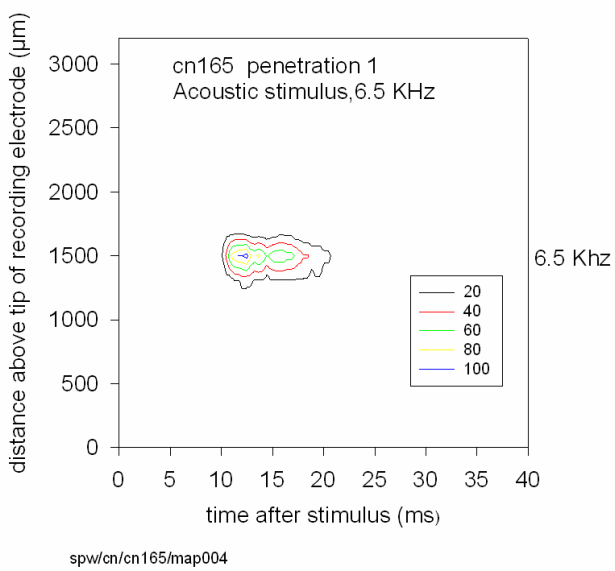


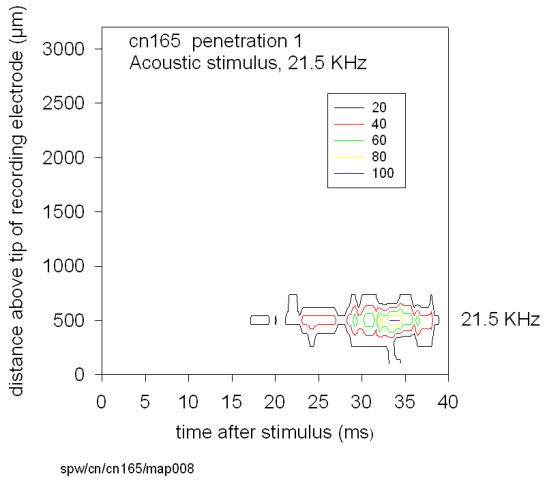


Figure 4

Figure 4 shows the response maps of the neural activity induced by the acoustic stimuli (tone bursts at 1/sec of three different frequencies, for penetration 1 into the ICC of cat CN165. Each map is the total of the responses to 30 successive tone bursts. The contour lines are scaled on the average maximum response (AMC) which is assigned an arbitrary value of 100. The beginning of the rising edge of the tone burst was at t = 0 on the abscissa. The response to low-frequency tones is somewhat broader and more transient.

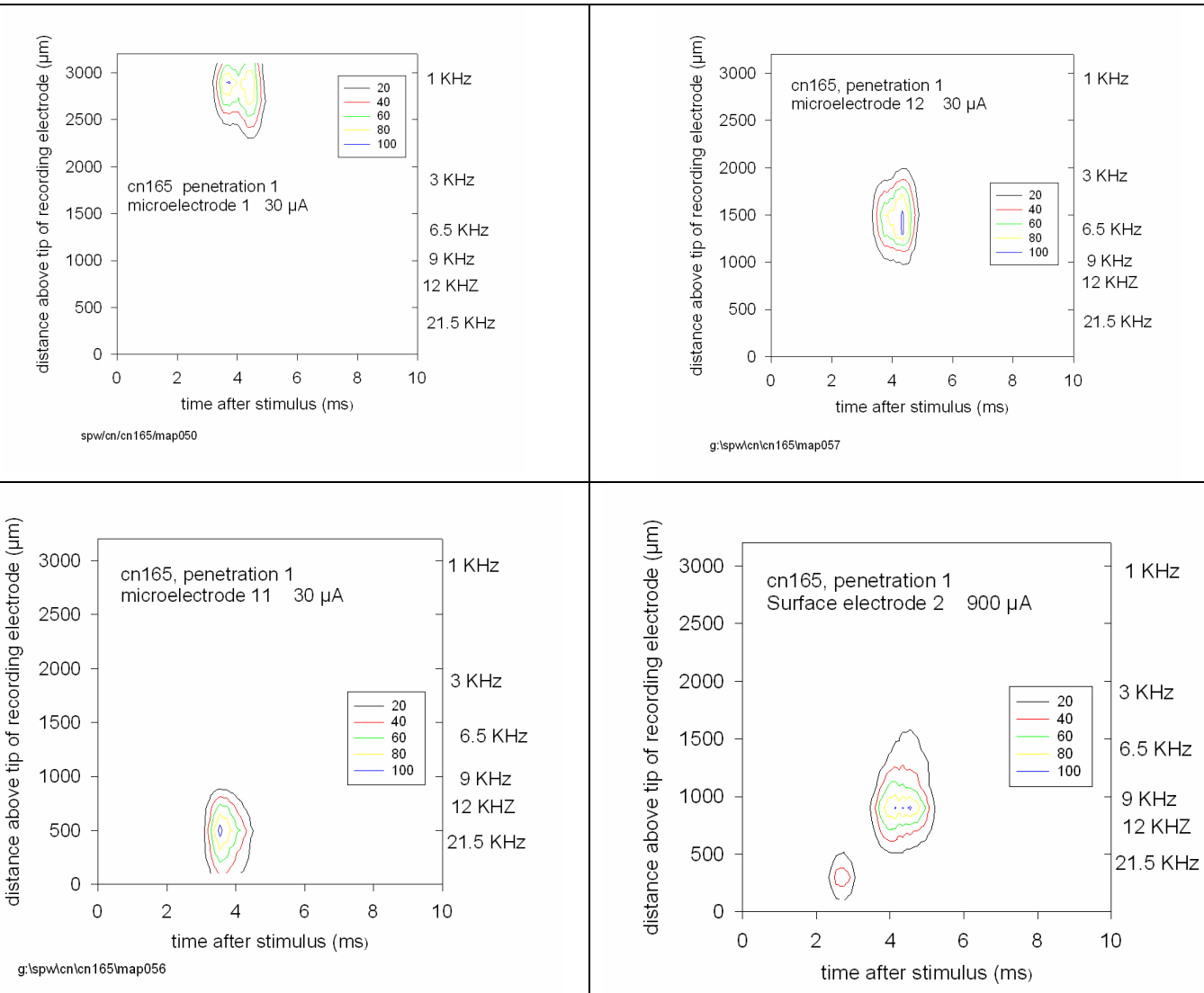


Figure 5

Figure 5 shows the response maps of the neural activity induced in the ICC by 3 of the microstimulating sites in the cochlear nucleus (2 on the caudal shanks and 1 on the rostral-lateral shank) and also by the surface electrode, on the dorsolateral surface of the cochlear nucleus. Much higher pulse amplitudes (400-900 µA) were required to induce multiunit activity via the surface electrode, but its activity focus was remarkably compact. However, the response map for the surface electrode shows 2 foci of activity with different latencies after the onset of each stimulus pulse, one shorter and 1 slightly longer than those of the microelectrodes on the rostral or caudal shanks. This indicates that the surface electrode was activating at neuronal pathways from the contralateral CN that was not being activated by the intranuclear microelectrodes.

For penetration 1 into the ICC, 10 of the microelectrodes and the lateral surface produced multiunit activity in the ICC with signal-to noise ratio >= 4 . Stimulating with the medial surface electrode induced marked activation of cranial muscles and a large EMG artifact, probably because of current spread into root or nucleus of the 7th cranial nerve, and so this electrode was not usable.

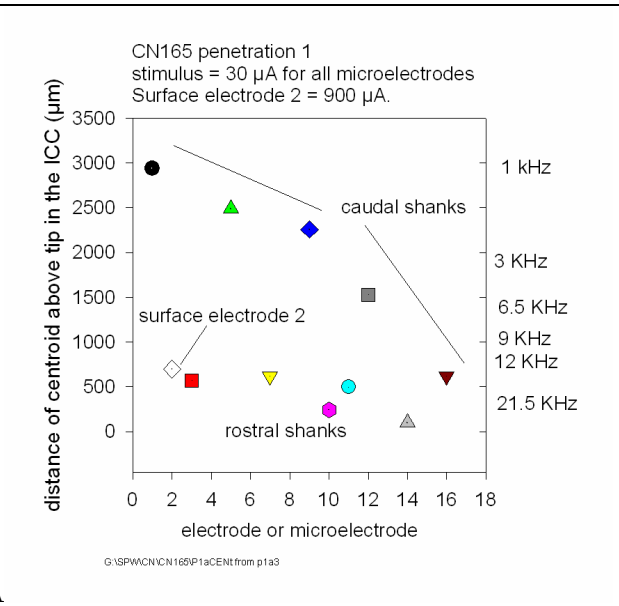
CN165 penetration 1
stimulus = 30 µA for all microelectrodes
Surface electrode 2 = 900 µA.
distance of centroid above tip in the ICC (µm)
3500
3000
2500
2000
1500
1000
500
0
caudal shanks
surface electrode 2
rostral shanks
1 kHz
3 KHz
6.5 KHz
9 KHz
12 KHz
21.5 KHz
0 2 4 6 8 10 12 14 16 18
electrode or microelectrode
G:\SPW\CN\CN165\P1aCENt from p1a3

A

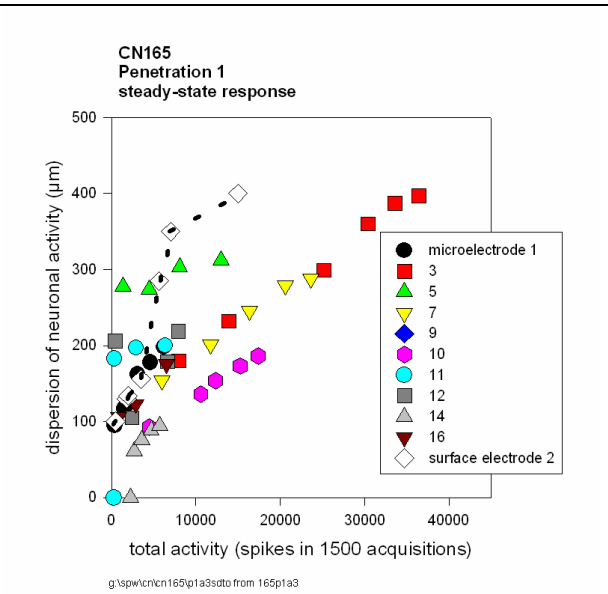
CN165
Penetration 1
steady-state response
dispersion of neuronal activity (µm)
500
400
300
200
100
0
0 10000 20000 30000 40000
total activity (spikes in 1500 acquisitions)
microelectrode 1
3
5
7
9
10
11
12
14
16
surface electrode 2
g:\spw\cn\cn165\p1a3sdto from 165p1a3

B

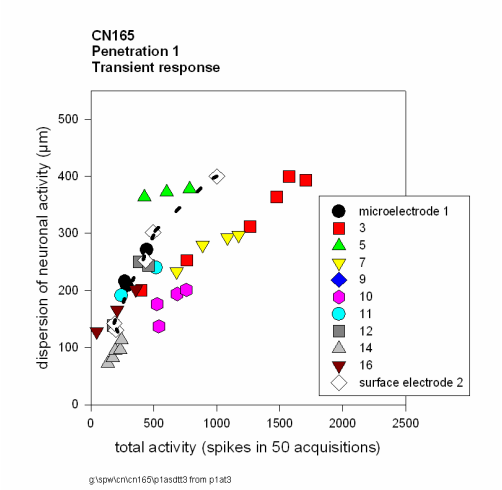
CN165
Penetration 1
Transient response
dispersion of neuronal activity (µm)
500
400
300
200
100
0
0 500 1000 1500 2000 2500
total activity (spikes in 50 acquisitions)
microelectrode 1
3
5
7
9
10
11
12
14
16
surface electrode 2
g:\spw\cn\cn165\p1asdtt3 from p1at3

C

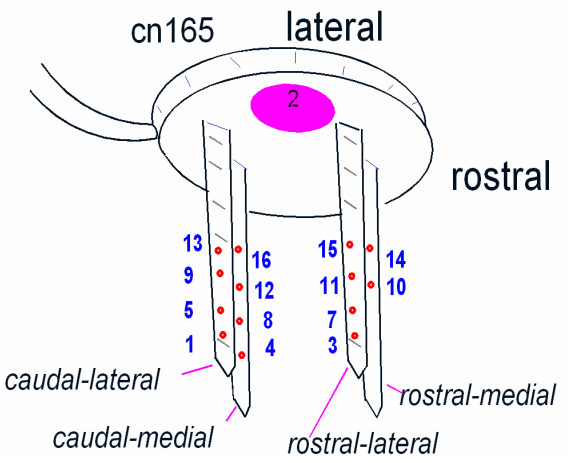
cn165
lateral
2
rostral
13
9
5
1
16
12
8
4
15
11
7
3
14
10
caudal-lateral
caudal-medial
rostral-medial
rostral-lateral

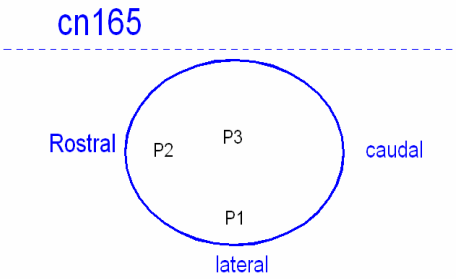
cn165
Rostral
P2
P3
caudal
P1
lateral

Figure 6

Figure 6A plots the depth coordinates of the centroids of the multiunit activity induced by the 10 microelectrodes and by the lateral surface electrode. The depth of the response maxima to acoustic tone bursts of different frequencies is indicated on the right ordinate. The centroids of the activity from the microstimulating sites on the caudal shank spanned the tonotopic gradient of the ICC from about 1 KHz to 20 KHz while the centroids of the activity from the sites on the rostral shanks were clustered in the high-frequency region. Figures 6B and 6C show the total multiunit activity plotted against the dispersion of the multiunit activity along the axis of the recording array in the ICC, for penetration 1, and for the steady state and transient responses, respectively. The multiple points for each stimulating site correspond to the total activity and dispersion of activity evoked at different stimulus amplitudes (10-30 μA for the microelectrode site, 400-900 μA for the surface electrode #2). The data points for the surface electrode are connected by the broken line. The ratio of dispersion of neuronal activity to total activity was lower for the microstimulating sites on the rostral shank of the CN array, but responses were concentrated in the high-frequency region of the ICC where absolute increments of frequency are compressed. In the lower part of the range of total activity, the ratio of dispersion of activity to total activity was similar for the surface electrode and most of the microstimulating electrodes, but when the total activity was greater (in response to higher amplitude stimuli), the ratio of dispersion/ total activity from the surface electrode became greater than that of any of the microelectrodes. The results were similar for the steady-state and transient responses (Figure 6B,C).

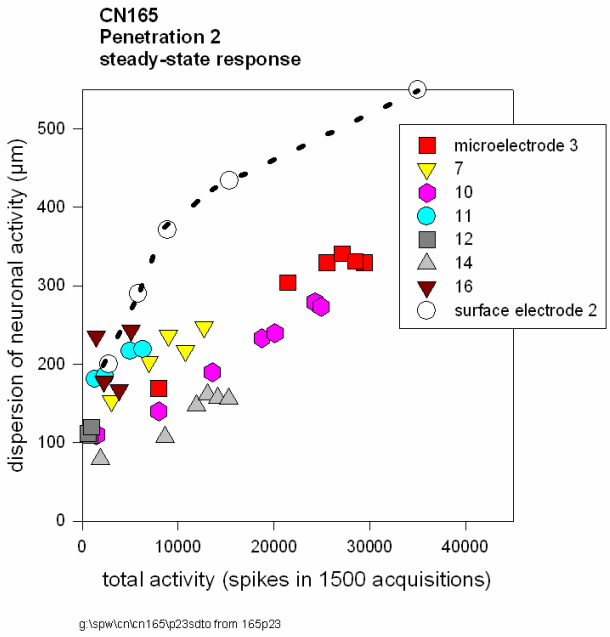


A

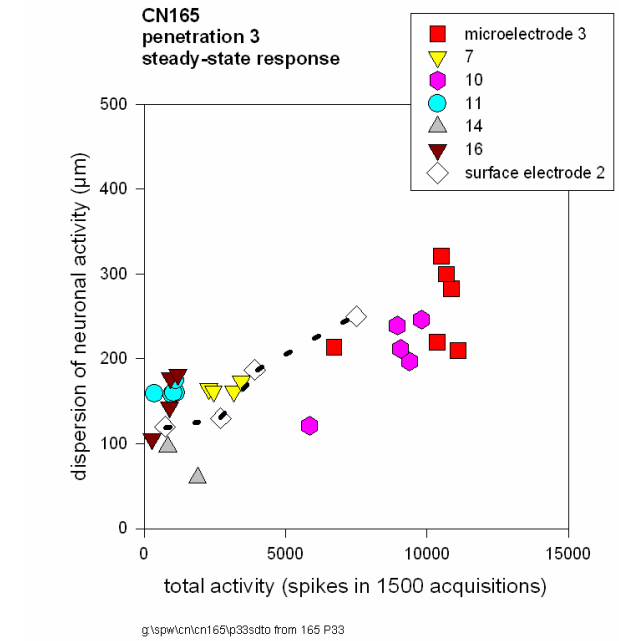


B

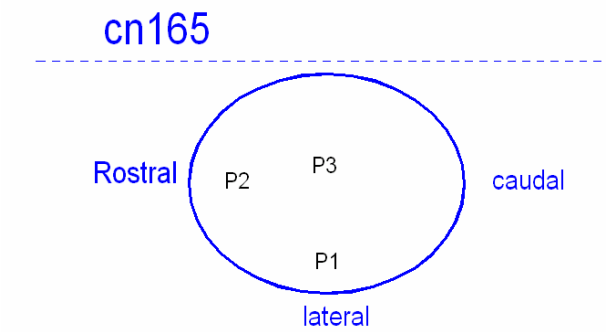


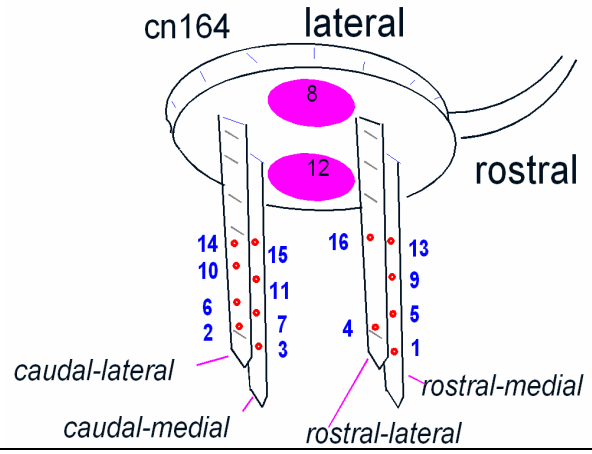


Figure 7

Figures 7A and 7B show the plots of total multiunit activity vs. dispersion of activity for penetrations 2 and 3 into the ICC of cat CN165. Penetration 2 was rostral and medial of penetration 1, and with the exception of site 16, all of the microstimulating sites that induced spikes with good signal-to-noise ratios were on the caudal shanks (another indication that the projections from the CN to each isofrequency lamina of the ICC are not uniform ). As in penetration 1, the microstimulating electrodes exhibited lower dispersion/ activity ratios than the surface electrode, over most of the range of total activity. However, for penetration 3, into the rostral-medial ICC, most of the same microelectrodes as in penetration 2 were represented, but the dispersion/total activity ratios were comparable for the microelectrodes and the surface electrode. In this respect, it is notable that the total activity induced by all of the electrodes was less that in the other penetrations, although the same range of stimulus currents was used.

In all of the penetrations, the time co-ordinates of the activity foci in the response maps was slightly different for the surface and microstimulating electrodes. For penetration 1, the post-stimulus latency was 3.93 ± 0.28 ms, vs 4.42 ± 0.17 for the surface electrode, which was significantly different ($p<.001$, 2-sided unpaired t-test). For penetration 3, the latencies for the microstimulating and surface electrodes were 3.96±0.65 ms and 5.03±0.81 ms, respectively ($p<.01$). This suggests that the surface

and microstimulating electrodes were at least to some extent activating different neuronal pathways from the cochlear nucleus to the ICC.

**Discussion**

It is notable that the individual microelectrodes spanned different portions of the range of total activity (for the range of stimulus amplitudes employed, 10-30 μA) This phenomenon appears to be related to the location of the site in the cochlear nucleus rather than the recording location in the ICC, since the microstimulating sites ranked similarly along the abscissa for all three penetrations into the ICC. Also, electrode site close together on one shank often spanned very different ranges with the same range of stimulus current, and in spite of the electrodes sites having very similar access impedances.

It is curious and noteworthy that in CN165, the microstimulating sites exhibited greater spectral selectivity that the surface electrode only when the stimulating electrode induced a lot of neuronal activity. This is the converse of what might have been expected if both type of electrodes were activating neurons deep in the ventral cochlear nucleus and quite distant from the surface electrode. At least part of the explanation may lie in the fact that the surface and microelectrodes electrodes apparently activate somewhat different neuronal pathways from the CN to the IC, and it is likely that the surface electrode were activating neurons close to the surface of the nucleus. In the rat and in the cat both the dorsal and ventral cochlear nuclei send tonotopically-organized projection to the central nucleus of the inferior colliculus (Malierca et al, 2005, Cant, 2003; Oliver, 1985). The feline dorsal cochlear nucleus also is organized tonotopically, with high acoustic frequencies represented dorsally and laterally and low frequencies represented ventrally and medially (Snyder et al, 1997). This tonotopic gradient would lie immediately beneath the surface electrodes, and thus would be accessible with good spectral specificity by electrodes on the surface if the CN.

In humans, and unlike in cats, the cochlear nucleus is overlaid by a thickened glia limitans and the neurons of the CN lie at least 0.5 mm below the surface of the brainstem. This spatial separation between the surface electrodes and the cochlear nucleus will increase the spread of the stimulus current, so the data from the cats would tend to show the spectral specificity of the surface electrodes in the most favorable light. It is also relevant that the dorsal and ventral nuclei probably subserve different functions, and that the DCN is primarily concerned with spatial localization of sound, particularly in elevation (e.g., Parsons and Voigt, 2001, Reiss and Young, 2005).

It is also instructive to compare the results from cat CN165 in this report with those reported in QPR #10, in which the stimulating arrays were implanted acutely, a few hours before the measurements in the ICC. For the acutely implanted arrays, the dispersion/activity ratios for the microstimulating electrodes were similar to those from CN165, but were much higher for the surface electrodes. The likely explanation is that the in the acutely implanted arrays, a thin layer of highly conductive cerebrospinal fluid between the surface electrode and the relatively non-conductive pia mater covering the cochlear nucleus allowed the stimulus current to spread laterally in the plane of the electrode, causing greater current spread within the nucleus. In CN165, the growth of the thin sheet of (less conductive) connective tissue under the array would reduce the opportunity for current from the surface electrode to spread laterally, and thus better confine the current field in the underlying nucleus.

**References**

J. G. Arenberg, S. Furukawa, and J. C. Middlebrooks, "Auditory cortical images of tones and noise bands," *J Assoc Res Otolaryngol*, vol. 1, pp. 183-94, 2000.

J. A. Bierer and J. C. Middlebrooks, "Auditory cortical images of cochlear-implant stimuli: dependence on electrode configuration," *J Neurophysiol*, vol. 87, pp. 478-92, 2002.

M. S. Malmierca, R. L. Saint Marie, M. A. Merchan, and D. L. Oliver, "Laminar inputs from dorsal cochlear nucleus and ventral cochlear nucleus to the central nucleus of the inferior colliculus: two patterns of convergence," *Neuroscience*, vol. 136, pp. 883-94, 2005.

J. E. Parsons, E. Lim, and H. F. Voigt, "Type III units in the gerbil dorsal cochlear nucleus may be spectral notch detectors," *Ann Biomed Eng*, vol. 29, pp. 887-96, 2001.

L. A. Reiss and E. D. Young, "Spectral edge sensitivity in neural circuits of the dorsal cochlear nucleus," *J Neurosci*, vol. 25, pp. 3680-91, 2005.

R. L. Snyder, J. A. Bierer, and J. C. Middlebrooks, "Topographic spread of inferior colliculus activation in response to acoustic and intracochlear electric stimulation," *J Assoc Res Otolaryngol*, vol. 5, pp. 305-22, 2004.

R. L. Snyder, P. A. Leake, and G. T. Hradek, "Quantitative analysis of spiral ganglion projections to the cat cochlear nucleus," *J Comp Neurol*, vol. 379, pp. 133-49, 1997.

## II: Activities at the house Ear Institute

### Introduction

To date, auditory brainstem implants each with an array of surface electrodes and an array of 8 or 10 penetrating microstimulating electrodes ("PABI" configuration) have been implanted into nine patients with Type 2 Neurofibromatosis. PABI patients 1, 2, 6 and 7 were tested during the last quarter. For comparison, five non-tumor (NT) ABI patients were tested in Verona, Italy, and three non-tumor ABI patients were tested in Hannover, Germany.

### PABI Threshold and Dynamic Range

Figures 1-4 show threshold and dynamic range measures for PABI patients 1, 2, 6 and 7, respectively. Within each figure, the threshold and maximum comfortable loudness level are connected by a vertical line for each electrode. Clusters of points show successive measures over time, with the most recent values at the right edge of each cluster. The initial 4-6 sets of points were collected at 3-month intervals and additional points were collected at longer intervals, typically 6 months or one year. Filled symbols present measures from penetrating microelectrodes and open symbols present measures from surface electrodes. Electrodes designated as "Surface L" (or "Surface R") are located along the left (right) side of the array as viewed face-on to the electrode contact surface and with the cable end pointing down.

PABI 1 (Figure 1) showed good stability over 3.5 years. Thresholds on both surface and penetrating electrodes increased by a factor of 2-3 over the first year and have shown excellent stability since. Only one penetrating electrode is useful for auditory sensations and the threshold for that electrode remains at about 2nC. The pattern of thresholds for surface electrodes suggests that the middle of the surface array is activating neurons immediately beneath the electrodes, but electrodes at the medial and lateral ends are simply spreading current to activate neurons near the middle of the array.

PABI 2 (Figure 2) also shows excellent stability in threshold measures for both surface and penetrating electrodes over more than 3 years.

Figure 1: PABI #1 Threshold and MCL

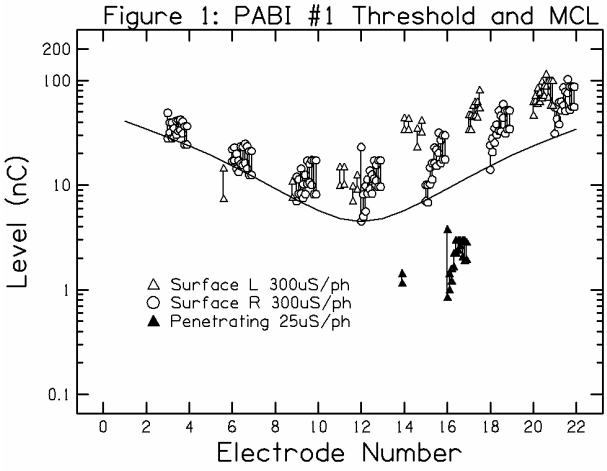


Fig 2: PABI #2 Threshold and MCL

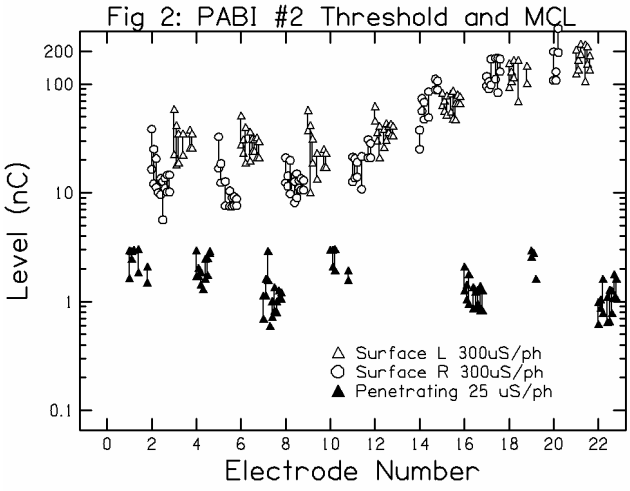

Threshold levels on penetrating electrodes ranged from 0.6 to 2 nC, while threshold levels of the surface electrodes ranged from less than 10nC to more than 100nC. The lateral end of the surface electrode array appears to be in the proper location while the medial end appears to be further away from stimulable neurons, leading to a rising threshold level at the medial end.

PABI 6 (Figure 3) continues to receive no auditory sensation from the surface electrodes and to receive unpleasant sensations in the ipsilateral face from stimulation with several of the penetrating electrodes. Several other penetrating electrodes produce only auditory sensations near threshold, but produce unpleasant sensations in the face when the stimulation level is raised. This is a curious finding, since the threshold levels of the penetrating electrodes are stable at 1 nC and lower, suggesting that these are indeed properly positioned within the cochlear nucleus, and thus should be far from any neuronal pathways that mediated pain. It is possible that the patient's brainstem had been markedly distorted by the tumor prior to its removal. This patient was only able to use one penetrating electrode in the speech processor due to the presence of nonauditory side effects (NASE) on all other electrodes.

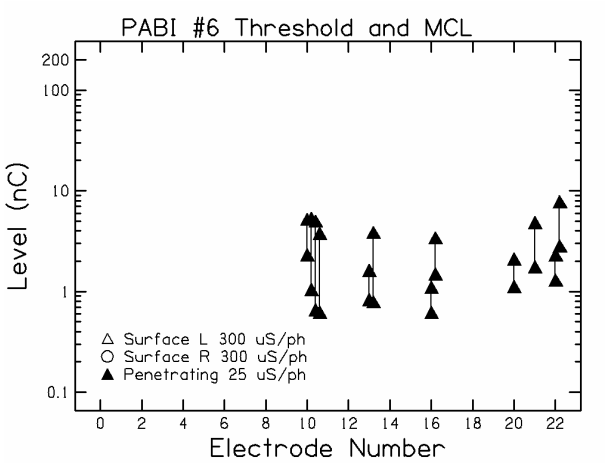


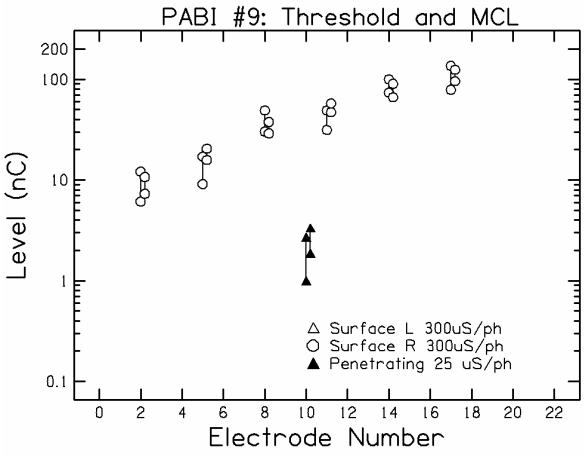


PABI 9 (Figure 4) was tested at the three-month follow-up period following initial activation in the last quarter. Only one penetrating electrode provided auditory sensations without NASE and its threshold level was in the expected range of 1-2nC. Surface electrode thresholds were stable over the testing period but the overall pattern was of thresholds that increased from lateral to medial suggesting that the lateral portion of the device was in a better location relative to auditory neurons.

**Threshold as a Function of Pulse Rate**

We continued to measure threshold levels as a function of pulse rate. Figure 5 presents the latest results from PABI patients 1, 2, 6, and 9 from this quarter, in addition to results from PABI 3 and 8 measured in the previous quarter. Open symbols show thresholds measured from surface electrodes and filled symbols show thresholds measured from penetrating electrodes. Note that four of the 6 PABI patients (1, 3, 6, 8) showed a pattern of increasing thresholds at low pulse rates, while two (2 and 9) showed no change in thresholds as a

function of pulse rate. In PABI patients in whom it was possible to measure thresholds for both surface and penetrating electrodes, the same pattern was observed for both: either no change as a function of rate (PABI 2) or decreasing thresholds as rate increased (PABI 3). The flat threshold pattern suggests that the integration time for threshold is quite short - less than 300us. If the biological/perceptual system were integrating the charge in the pulses over more than 300us then the thresholds at high stimulation rates would be lower. However, the sloping threshold functions suggest a very long integration time of 100ms or more. Thresholds decreased when the time between stimulation pulses decreased from 100ms (10Hz) to 50ms (20Hz). In PABI 3 and 6 (middle two panels in Figure 5) it appeared that the threshold curves flattened out at these low rates, with little difference in threshold between 10 and 20Hz. In these subjects the portion of the function that is flat is more difficult to explain. If there is an integration time window, increasing the stimulation rate from 100Hz to 1000Hz increases the amount of energy in that window by a factor of 10, yet threshold is not changed. The flat portion of these functions may reflect a "leaky" integrator, where excess charge beyond some baseline level is ineffective or "bleeds away" and does not contribute to threshold. The shape of the curves does not appear to be correlated with speech recognition performance as both flat and sloping curves have been found in non-tumor ABI patients who span a range of performance (see progress report #10 ). We will continue to collect threshold measures as a function of stimulation rate in PABI and ABI patients, both NF2 and non-tumor.

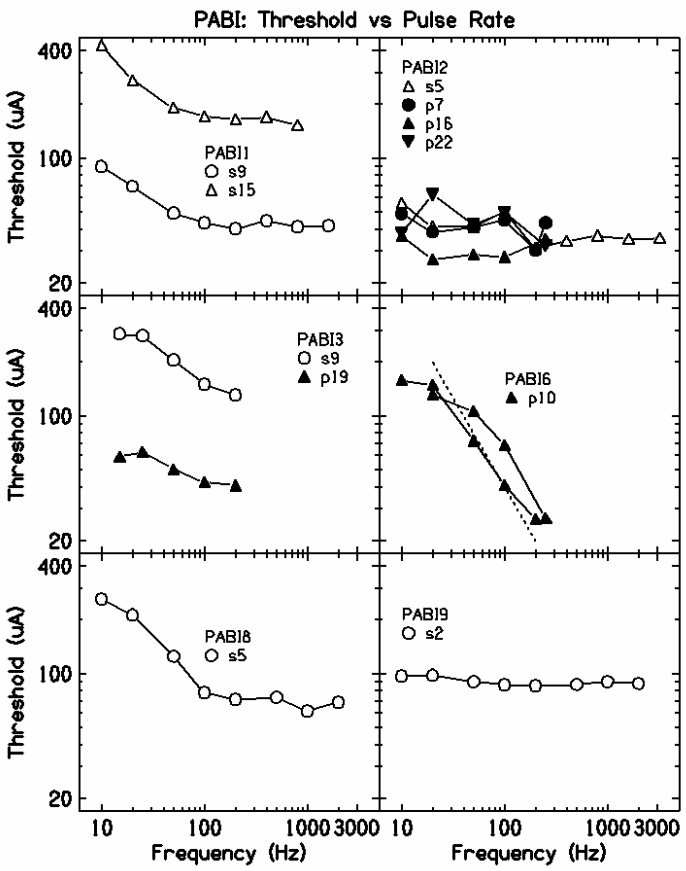


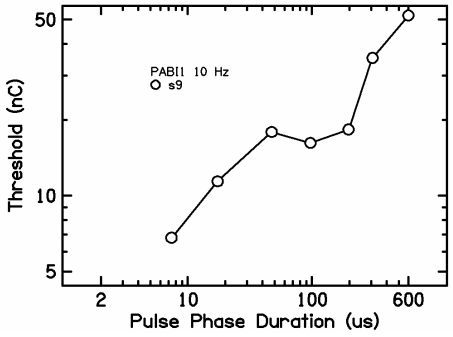


**Threshold as a Function of Pulse Phase Duration**

Previous measures of threshold as a function of pulse phase duration have shown functions that

decreased in terms of charge/phase as pulses became shorter (see previous progress reports). The shortest pulses are most efficient in that they inject the least amount of charge at threshold There was no indication of the functions "bottoming out" at short pulse durations - thresholds continue to drop down to 2us/phase. Figures 6 and 7 present measures of threshold obtained during the last quarter for PABI patients 1 and 6, respectively. Figure 6 presents data from PABI 1, for a surface electrode. There is a dip in the function for pulse phase durations of 100-200us, but in general the function continues to decrease with decreasing pulse duration, down to the shortest pulse duration measured. Figure 7 presents measures from PABI 6, for a penetrating electrode. The two functions represent measurements from two different testing sessions, and so indicate the test-retest reliability of the measures. Again, thresholds decreased with decreasing pulse phase duration, down to 2us/phase.

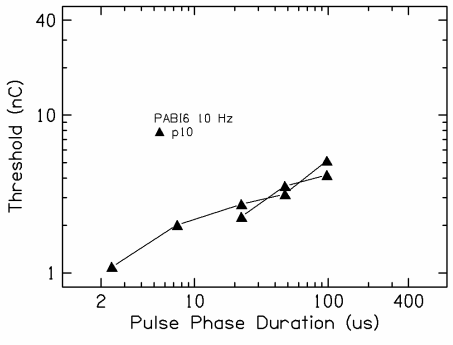


**Adaptation (SIDNE)**

Physiological experiments with penetrating electrode stimulation showed evidence of a strong adaptation effect, termed Stimulation-Induced Depression of Neural Excitability (SIDNE). We assessed SIDNE in PABI 6 by presenting a 30-second stream of pulses at different stimulation rates and instructing the patient to report the loudness every 5 seconds on a scale of 0 to 10. Figure 8 presents the results for three stimulation rates: 100, 200, and 250Hz. Little adaptation was observed at any stimulation frequency. Loudness started at an initial value of 5 or 6 (on a scale of 0-10) and declined slightly to values of 5 or 4.5 respectively after 5-10 seconds of continuous stimulation.

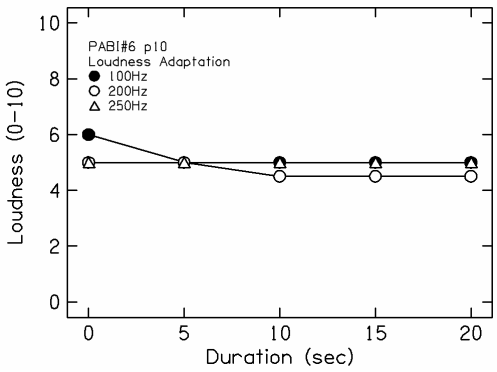


**Pulse Rate Discrimination**

One possible advantage for penetrating electrodes was thought to be the activation of a small population of neurons, possibly including neurons with good properties for processing temporal information. We measured pulse rate discrimination as an indicator of the perceptual ability to discriminate small time intervals. A standard pulse rate was presented and compared to a higher rate. We measured the percent change necessary to produce 79% correct discrimination. Figure 9 presents the results of

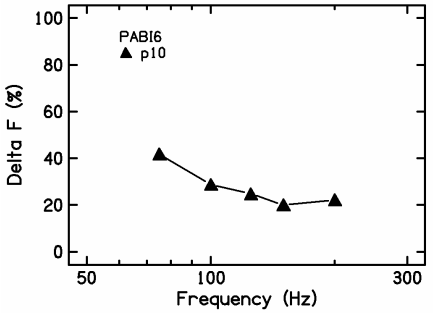

this measurement for PABI 6 for a penetrating electrode, as a function of the standard rate. This patient was able to discriminate a rate change of about 20% based on pitch over the range of standard rates of 100 to 210Hz. We did not test standard rates higher than 210Hz due to concerns about SIDNE. At the highest rate tested this level of discrimination indicates that this patient could discriminate time intervals that differed by 1ms (4 vs 5ms period). Considerable variability has been observed in this measure, with cochlear implants typically able to detect 7-10% rate differences up to standard rates of 250-300Hz. Some ABI patients require 30-50% difference in rate for discrimination and can only perform the task up to standard rates of 150Hz. Overall, the results from PABI 6 on this penetrating electrode were intermediate between the best performance and the poorest performance of other ABI patients..

**Speech Recognition**

Standard speech tests measured speech recognition performance on vowels, consonants, sentences in sound alone and sound plus lipreading conditions. Figure 10 presents the results over time for all PABI patients. There is no clear trend for scores to increase over time. Note that the scores for open set sentence recognition without lipreading (lower right panel) are all at 20% correct or lower. This level of performance is similar to that seen in regular surface electrode ABI patients.

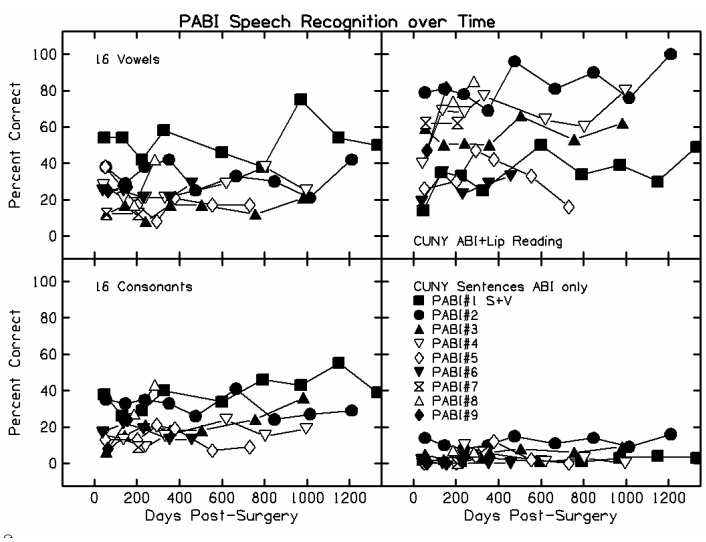


**Presentations:**

Shannon RV (2007). "Ear and brain: Organization of sensory cues into complex objects", Assoc Res Otolaryngol Midwinter Meeting, Denver, Feb 10-15.

Shannon RV, McCreery D, Colletti V, Lenarz M, Lenarz T and Lim H (2007). "Speech recognition and psychophysical results from electrical stimulation of the human cochlear nucleus and inferior colliculus", Assoc Res Otolaryngol Midwinter Meeting, Denver, Feb 10-15.

Shannon RV (2007). "Speech recognition and psychophysical results from electrical stimulation of the human cochlear nucleus and inferior colliculus", Grand Rounds/Neuroradiology Conference, St Vincent's Hospital, March 23.